Proceedings of ERAD (2002): 84–89 © Copernicus GmbH 2002

ERAD 2002

Fall velocity and axial ratio of snowflakes

R. Schefold, B. Baschek, M. Wüest, and E. Barthazy

Institute for Atmospheric and Climate Science, ETH, 8093 Zürich, Switzerland

Abstract. In this work, we describe a method for optical snowflake measurements. The method is used in field campaigns to collect snowflake data of different crystal types and riming degrees and includes a statistical evaluation and presentation of the data. The instrument is capable to measure size, shape, and fall velocity of individual particles. The optical measurement area consists of two vertically offset measuring planes. The images of the particles have to be matched with a matching program. The matching process includes the recognition of shape information of particles, the matching of particles and a shape correction. The data is statistically evaluated. Particle data of time intervals is binned into fall velocity vs. size bins and axis ratio vs. size bins. Quantiles describe the scatter of the variables, whereas power laws describe the average dependence of the variables on the diameters. An example shows a clear dependence of particle fall speeds on the riming degree in accordance to literature. The fall velocity distribution depends partially on the particle density which is increased due to the riming. The measurements include a specification of the spread of the measured fall spread, e.g. 50% of unrimed dendrites have a fall velocity, which is more than 0.22 m/s different from the median value in the corresponding size class. Fall velocity scatter increases vs. size. Another example shows a different and clear axis ratio behaviour of 1-dim and 2-dim growing particles. 2-dim growing particles have a constant axis ratio, whereas 1-dim particles show an decreasing axis ratio vs. size. For both, the 1-dim and 2-dim particles, the scatter decreases vs. size.

1 Introduction

The properties of snowflakes such as their size distribution, fall velocity or axial ratio are important for several purposes. The knowledge of accurate fall velocities and its spread, e.g. can be used to calculate aggregation rates in modelling precipitation processes. The size distribution and especially the particles axial ratios can provide information for the interpretation of returned radar power, in particular of polarized radar (Vivekandan et al., 1993, Fabry and Szyrmer, 1999).

Except for some in situ techniques, where snowflakes are captured and examined, optical techniques are the choice when snowflakes are to be investigated. However, accurate experimental observations of size distributions, fall velocities and axial ratios with description of the true spread of each property (e.g. within a size class) are scarce due to either the limited number of observed snowflakes, or to the limitations of the observations techniques (Locatelli and Hobbes, 1974, Zikmunda, 1972).

To overcome these limitations, an optical spectrometer was developed at the ETH Zurich. The instrument is capable to measure several properties like the real time-dependent size distribution in the range of 0.65–70 mm or axis ratios and fall velocities of single hydrometeors.

This optical spectrometer is used in ongoing field campaigns to collect snowflake data of different crystal types. One snowfall event of a few hours can yield data of several tens of thousands of snowflakes. In addition, ice crystals are replicated (Formvar) regularly with time intervals of about 10 min to determine their habit and riming degree. The studies show on a statistical base the dependency of the fall velocity and the axial ratio on the size of the snowflake, but also on the type of snow (crystal type, riming degree).

2 Setup

Two mountains – Mount Rigi and Mount Uetli, Switzerland – were chosen as measuring sites for this analysis, which have a steep rising front pointing towards the lowlands and the main weather direction. The setup, as seen in Fig. 1, is identical at both mountains and is split up in two locations – one at the bottom and one close to the top. The steepness of the mountains allows to measure variables at different height levels at similar horizontal position. At the bottom station, a vertically pointing X-band radar is used, which is described in Baschek et al., 2002. At the top station the optical spectrometer is used, which is described briefly in the next section. A more detailed description can be found in Barthazy and Schefold, 2001. In addition, Formvar probes (Schaefer, 1956) were taken at the top station to determine ice crystal types and riming degree.

Correspondence to: R. Schefold
(schefold@atmos.umnw.ethz.ch)

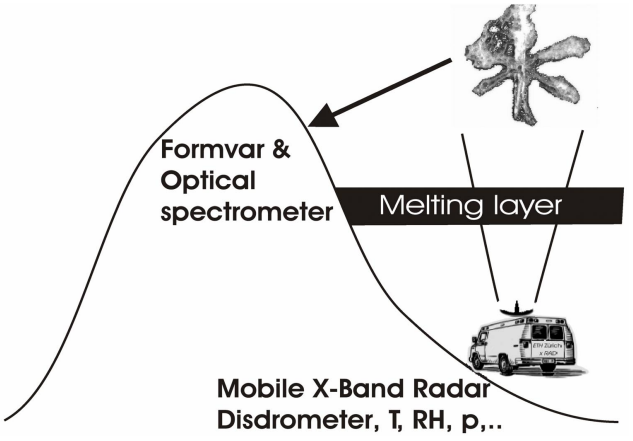

Fig. 1. Schematic drawing of the setup with two locations, one at the bottom and the second close to the top of the respective mountain.

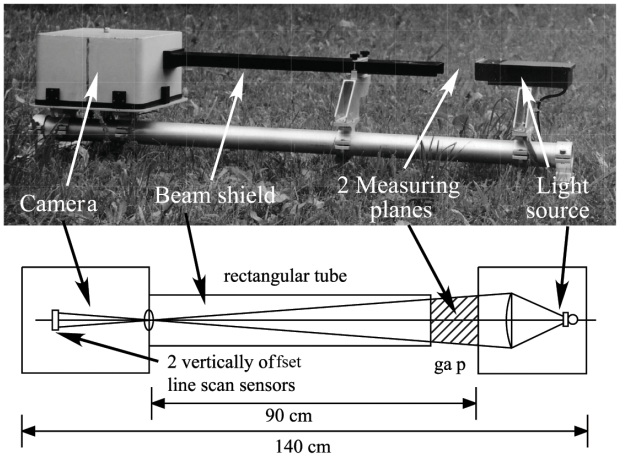

Fig. 2. Side and top view of the sensor unit.

3 Optical spectrometer

A light source is producing a beam of uniform parallel light directed towards an electronic line scan camera. The optical path of the beam is shielded by a rectangular tube except for a gap of 108.5 mm length near the light source. Precipitation particles falling through the light beam in this gap cast a shadow, which is measured by the line scan camera. The camera is sensitive in two horizontal planes having a vertical distance of 9.45 ($\pm$0.55) mm. The length of these measuring planes is given by the dimension of the gap of the housing, the width is given by the dimension of the line scan sensors in the camera and was determined to be 76.75 ($\pm$4.25) mm. A top and a side view of the sensor unit are shown in Fig. 2.

4 Matching software

Due to the two scan lines, every particle is recorded twice. To calculate the fall velocity of the particle, the two images of the particle have to be identified and matched (Barthazy and Schefold, 2001).

The main idea of the matching process is to compare every image of a particle taken in the upper line scan with every image taken in the lower line scan within certain time frames (blocks). Excluded from comparison are images, which touch the border of the block or whose spatiotemporal distance to its comparison partner is larger than a cut-of value. The comparison is done by a set of shape describing characteristics (height h, width w, circumference c, number of pixels n and greyscale $g = n/h \cdot w$) of the images. For every couple of images (i, j) a number $Z_{i,j}$ is calculated, which describes the quality of a possible match for the upper i-th image with the lower j-th image:

$$Z_{i,j} = \left(\frac{\min(h_i, h_j)}{\max(h_i, h_j)}\right)^{f_h} \times \left(\frac{\min(w_i, w_j)}{\max(w_i, w_j)}\right)^{f_w} \times \dots \quad (1)$$

with $0 < Z_{i,j} < 1$ and where i indicates characteristics taken in the upper, j in the lower beam. $f_h, f_w, \dots$ are empirically chosen weighting factors.

Not only the shape of the images is compared. In addition, a list is carried on including the horizontal movement of the last ten already matched particles. Therefore, an average horizontal movement is also known. The horizontal movement of each couple (i, j) is compared with the average value of that list. If the variation is larger than a certain cut-off value, a match of that potential couple is forbidden by setting $Z_{i,j}$ to zero. A recursive search finds a best general assignment within all spare entries $Z_{i,j}$. This general assignment is then equivalent to a match of upper images with lower images within the block.

Another task of the program is about the reshaping of the images which is computed after the matching process completed and after the movement of the particles are known. There are two cases:

Stretching: Due to the constant scan rate the shape of the image of a particle does not need to have the shape of the particle itself, e.g. the higher the fall velocity of a particle is, the less times it will be scanned and the image will be compressed vertically. Similarly, a small fall velocity will result in vertically stretched images due to more scans of the particle. We may call this effect "stretching due to velocity". The fall velocity threshold is at 1.435 ms^{-1}, at which the images are not distorted vertically. This threshold value is given by the scan frequency. Because the precise fall velocity is known due to the matching process, the vertical stretching of the image can be corrected: The *elongation*, on one hand, is done by doubling of certain lines. The *truncation*, on the other hand, can not be done by deleting lines, because loss of shape information has to be avoided. Instead, the length of the lines is accordingly increased. This corresponds to the application of a zooming factor to the original particle shape.
Shearing: The other effect has its reason in the horizontal movement of particles in the measuring area, e.g. due to horizontal wind. If the movement of the particle has a compo-

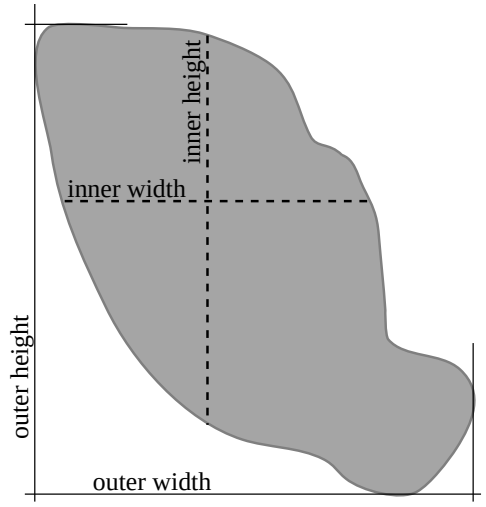

Fig. 3. Definition of the calculated dimensions of a particle.

nent parallel to the line scan cameras, then the shadowed area will shift from scan to scan. The resulting image of the particle will be sheared. We may call this effect "shearing due to horizontal movement". Normally both effects, the stretching and the shearing, cumulate on each particle. The program shifts back each line under the assumption that the shift between scan lines is a linear part of the complete shift of the particle between the two scan planes.

The last task of the matching program is then to print out (a) the corrected geometrical information of every matched particle as shown in Fig. 3, (b) the horizontal and vertical movement information and (c) flags, which indicate the quality of the computed match.

5 Data evaluation

The matching software calculates for almost every particle shape- and movement information. The in-situ measurements include a particle habit and riming degree typing, which is done with the help of Formvar probes. If the falling particles remain of the same habit and riming degree for at least several minutes, the gained individual movement and shape information is plotted against the particle diameter. Figures 4a and 4b show particle fall velocities, whereas Fig. 5 shows axis ratios. There exist several ways to explain the diameter of particles: e.g. the inner width (height) of a particle is defined as longest horizontal (vertical) line, completely enclosed in the image of the particle. The outer width (height) is the width (height) over all. If the particle has an oblate orientation, inner and outer width are equal. The axis ratio is defined as ratio of inner height width and is depending on both the orientation of the particle in space and an particle intrinsic axis ratio. The axis ratio can inform about the oblateness of a particle.

The particles of the corresponding time interval are binned into size and velocity resp. size and axis ratio bins. The

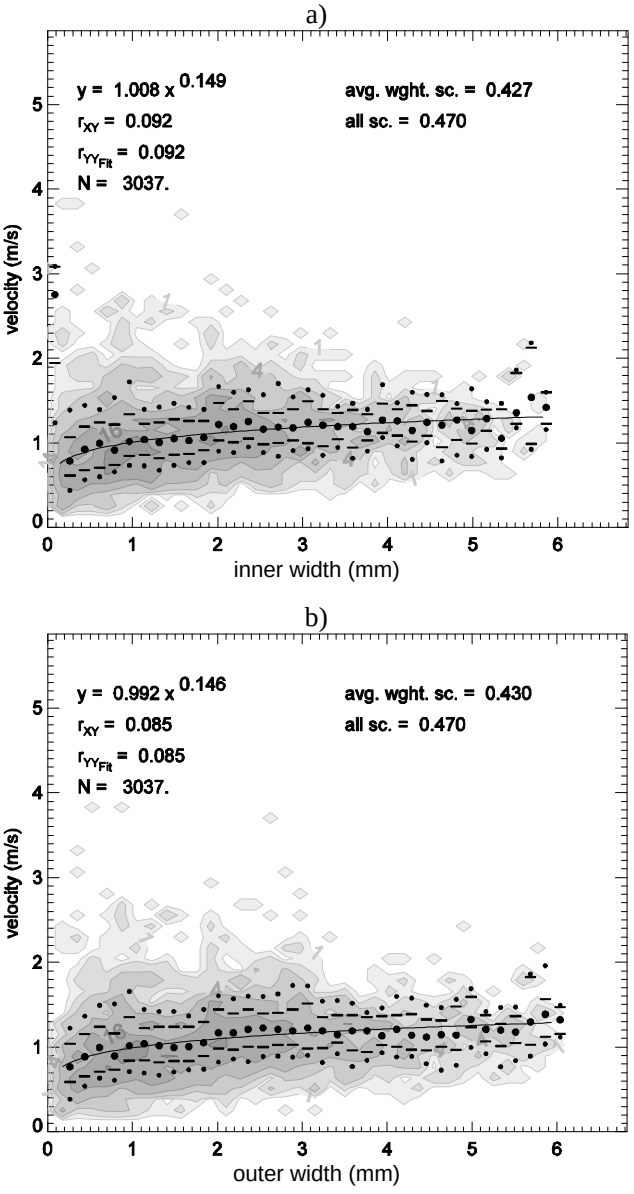

Fig. 4. Data from 24 Mar 2002, 00:40–02:00, at Mt. Rigi. **(a)** Measured fall velocity vs. inner width of particles. **(b)** Measured fall velocity vs. outer width.

greyscale shows the occupation of the bins: Each greyscale step corresponds to a factor two. In every size class, five quantiles are designated ($\cdot 12.5\%$, -25%, $\bullet 50\%$, -75% and $\cdot 87.5\%$) to indicate the scatter of the variable, e.g. for modelling purposes. An "average weighted scatter" ($avg.wght.sc.$) indicates an average weighted band between the 25% quantiles $(qi(25))$ and the 75% quantiles $(qi(75))$, which is given in y-axis dimension:

$$avg.wght.sc. = \frac{\sum_{i}^{sizeclasses} \left(\left(q_i\left(75\right) - q_i\left(25\right) \right) \cdot n_i \right)}{\sum_i n_i} \qquad (2)$$

The $avg.wght.sc.$ is dominated through the differences of

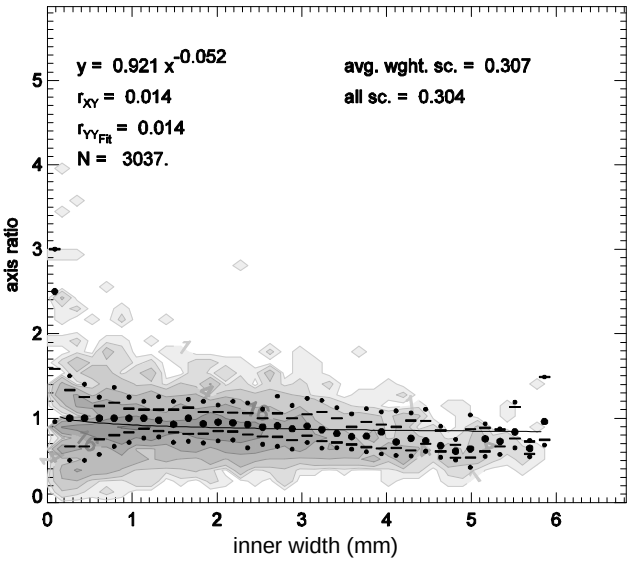

Fig. 5. Data from 24 Mar 2002, 00:40–02:00, at Mt. Rigi. Axis ratio vs. inner width.

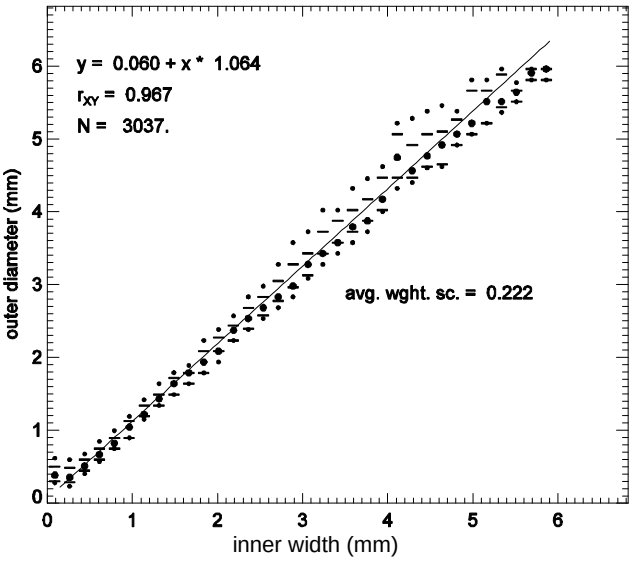

Fig. 6. Data from 24 Mar 2002, 00:40–02:00, at Mt. Rigi. Outer width vs. inner width.

the quantiles in highly occupied regions. An "overall scatter" ($all\ sc.$) indicates a difference between a general 75% quantile $(q(75))$ and a 25% quantile $(q(25))$:

$$all\ sc. = q(75) - q(25) \tag{3}$$

which is broader than $avg.wght.sc.$

It is generally acknowledged that power laws can be specified as parameterisation for fall velocity vs. size relationships. With power laws, it is easily possible to calculate DSD moments (e.g. drop count, water content or reflectivity). In this work, power laws are also specified for axis ratio vs. size relationships. These can be used as a parameterisation in the polarized radar field. Moreover, the linear correlations r_{XY} and $r_{YY_{Fit}}$ are given, which indicate on a double logarithmic scale the linear correlation of the XY-data itself and the fitted $r_{YY_{Fit}}$ data. The correlations r_{XY} and $r_{YY_{Fit}}$ are equal, if power laws are fitted onto the data.

Figures 4a and 4b show fall velocities vs. inner width and outer width, respectively. The occupation of the bins, the quantiles and the fits show no significant differences. This is endorsed through Fig. 6, where the outer width vs. the inner width is plotted. The fit line shows that the outer width is only slightly larger than the inner width. We use the inner width as particle diameter in this work: Both, the correlation coefficient and the average weighted scatter seem to be slightly better.

6 First results

6.1 Riming on dendrites

Several case studies have been taking place in winter season 2001/2002. On 23 March 2002 a case was observed at Mt. Rigi (Baschek, 2002), where Formvar probes show mostly dendrites. The crystal classification was done after Magono and Lee (1966). Meanwhile, several riming degrees were observed at different times. The riming degree classification was made after Mosimann et al. (1994). The classification is build on a 6-ary scale, which has values from 0 to 5. Particles with a riming degree 0 are unrimed (no frozen cloud droplets at the surface or the ice crystal), whereas particles with a riming degree of 3 are densely rimed (whole surface covered with one layer of frozen drops; clear identification of the crystal shape possible; several layers of frozen drops only at the edges of a plate like crystal) and particles of degree 5 are graupel particles (all type of graupel like conical, hexagonal, or lump). Figures 7a, 7b and 7c show fall velocity distributions for particles with an average riming degree of about 0.5, 3.0 and 4.5. With an increasing average riming degree is a clear distinction of the distribution to higher fall velocities recognizable. The fitted power laws are $v = 0.9 \cdot D^{0.2}$ (for riming degree 0.5), $v = 1.2 \cdot D^{0.2}$ (for riming degree 3.0) and $v = 1.3 \cdot D^{0.6}$ (for riming degree 4.5). The increase is explained by an increase of the density of the particles due to the cloud droplets. The fall velocity distributions of particles with average riming degrees of 0.5 and 4.5 are compared with corresponding data form Locatelli and Hobbs (1972), where a good agreement between the fit lines and the reference relationships could be found.

In Figure 7a, the highest occupation of the measured fall velocities is in the size regime of 2.6 mm to 3.2 mm. The median values are almost constant in the regime of 1.8 mm to 3.2 mm, but the quantiles of the distributions show a broad scatter of measured fall velocities in most size classes. The average weight scatter in Fig. 7a is 0.44 m/s. This scatter increases the probability for aggregation within the same size class and/or for aggregation between neighbouring size classes with similar median fall velocity values. In the field

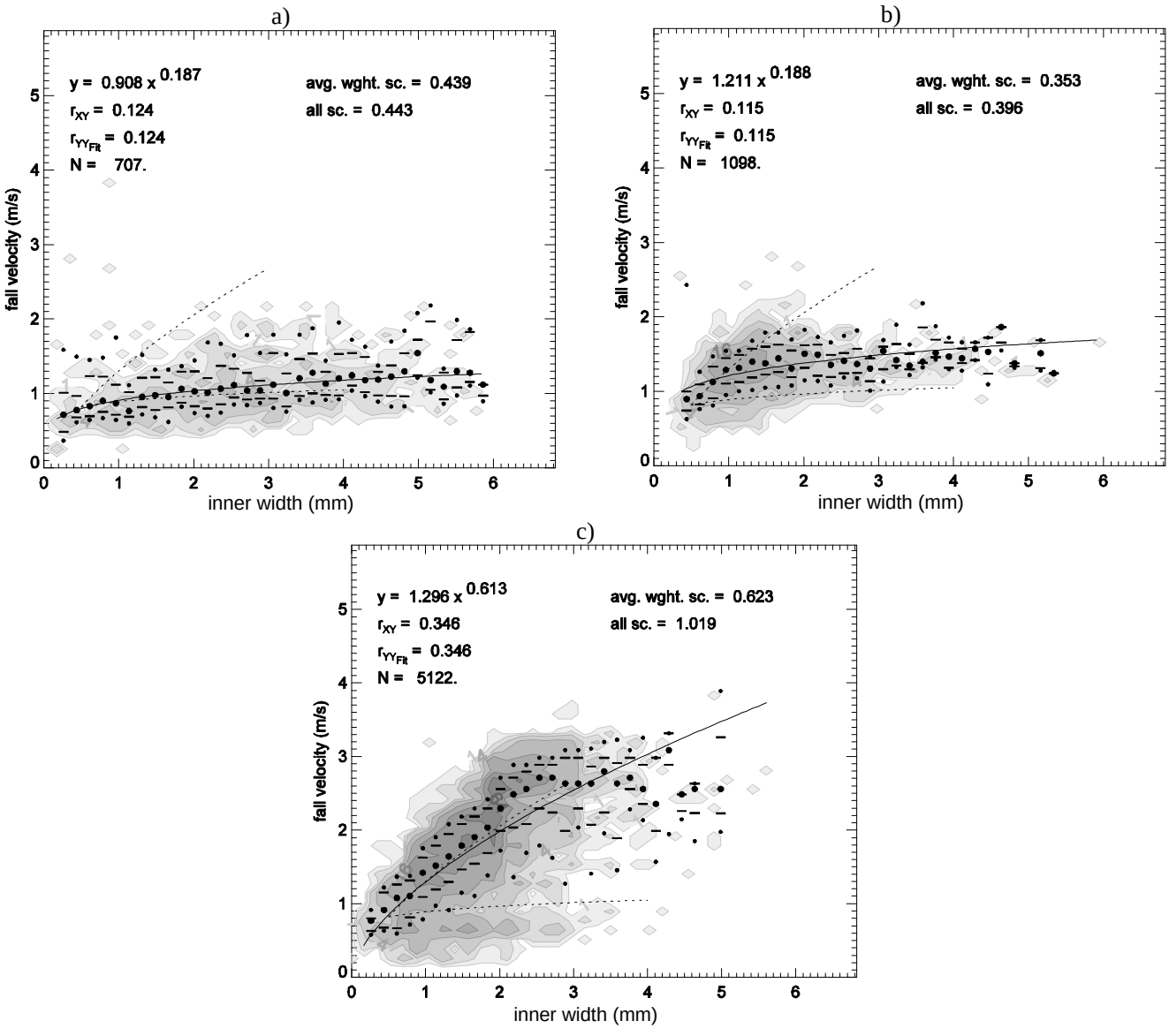

Fig. 7. Measured fall velocities vs. inner widths of observed particles. The particles were of dendritic habit. Data from 23 Mar 2002 at Mt. Rigi. In each panel, two reference lines are drawn (dashed, after Locatelli and Hobbs, 1974) with $v = 1.3 \cdot D^{0.66}$ for lump graupel (upper line) and $v = 0.81 \cdot D^{0.16}$ for unrimed aggregates (lower line). **(a)** Particles were almost not rimed (Riming degree about 0.5 at 15:00–15:25). **(b)** The whole surface was with one layer of cloud droplets covered. At the edges were several layers observed (riming degree about 3.0 at 18:18–18:35). **(c)** The whole surface was with several layer of cloud droplets covered (riming degree about 4.5 at 18:36–18:46)

of precipitation modelling, usage can be taken from the information of increased aggregation probability to calculate aggregation rates.

6.2 Axis Ratios

On 6 February 2002, 17:30-17:40, needles and aggregates of needles (type N hereafter) were observed, whereas on 23 March 2002, 18:40–22:05, dendrites and aggregates of dendrites (type D) with a riming degree average of 2.5 and a riming degree span of 1 to 5 were observed. In Fig. 8, axis ratios for these two particle types are shown. The axis ratio is defined as inner height/inner width (Fig. 3) and is depending on the orientation and the shape of the particle in space and gives information on the oblateness of the particle. For comparison purposes power laws are fitted to the data. The type N particles show an axis ratio which is dependent on the size of the particles (fitted power law for axis ratio $\varepsilon = 0.8 \cdot D^{-0.2}$), whereas most values of the axis ratios of the type D particles are in the axis ratio region of 1 (fitted power law for axis ratio $\varepsilon = 0.9 \cdot D^{0.03}$). For both distributions, the scatter of the axis ratio is decreasing to larger diameters.

For small particle sizes, the scatter of the axis ratio values (distance between the 25% quantiles and the 75% quantiles)

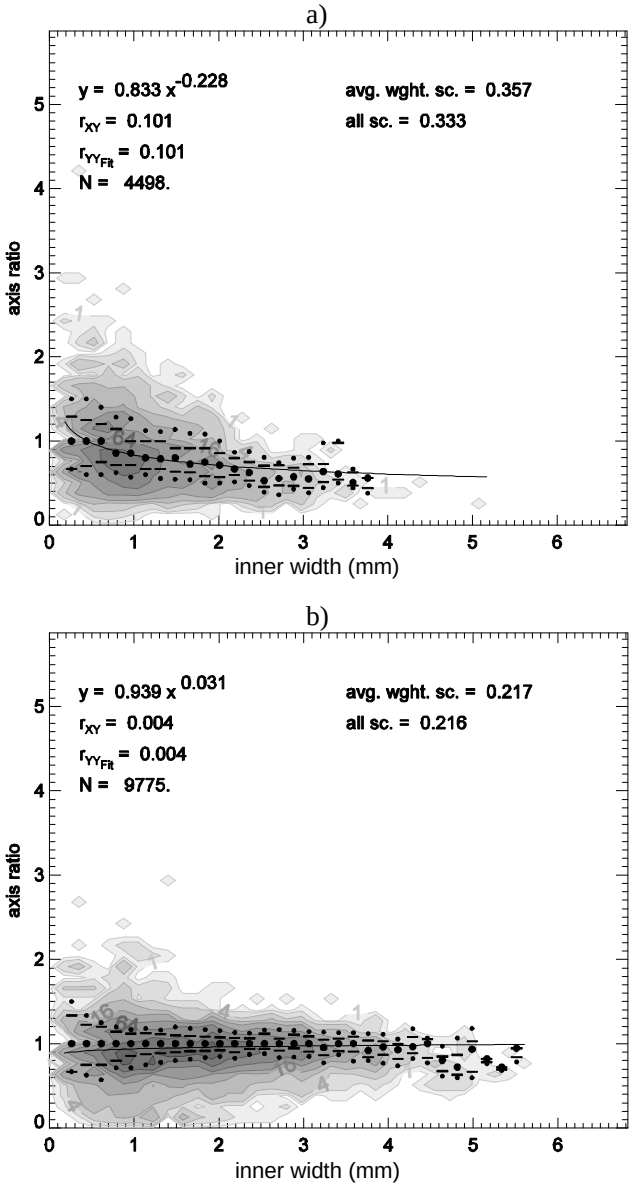

Fig. 8. Measured axis rations vs. inner width of particles. **(a)** Axis ratios of unrimed needles and aggregates of them. Data from Mt. Rigi, 06 Feb 2002, 17:30-17:40. **(b)** Axis ratios of dendrites and aggregates of dendrites with a riming degree of avg. 2.5 and a riming degree span of 1–5. Data form Mt. Rigi, 23 Mar 2002, 18:40–22:05.

is 0.6, resp. 0.7, and the median value is for both 1. For large particle sizes, type N particles level at an axis ratio value of 0.55, whereas the dendrites level at an axis ratio value of 1. An explanation for this clear difference of axis ratios at large sizes is, that the type N particles are 1-dim growing, while the type D particles are 2-dim growing.

7 Conclusions

Accurate fall velocities of particles are described by quantiles, which express the scatter of the variables, and power laws, which explain the average dependence of the fall velocity on the diameter.

There exist several ways to explain the diameter of particles, e.g. the inner width of a particle is defined as longest horizontal line completely enclosed in the image of the particle. Both, the correlation coefficient of the data and the average weighted scatter seem to be better, if using an inner width than using an outer width.

The median fall velocity values of dendrites with increasing average riming degree correspond well with literature data and show an expected increase of the distribution to higher fall velocities.

However, the fall velocity vs. relationship for unrimed dendrites (usually a power law) has a comparatively flat appearance. But still, 50% of the particles have a fall velocity, which is more than 0.22 m/s different from the median value in the corresponding size class. The scatter of the fall velocity distributions is increasing vs. size. This scatter increases the probability for aggregation within the same size class and/or for aggregation between neighbouring size classes with similar median fall velocity values.

The axis ratio of a particle is defined as inner height/inner width of the particle and can give information on its oblateness. Observed 1-dim growing particles (needles) and 2-dim growing particles (dendrites) show a different and clear axis ratio behaviour. The observed 2-dim growing particles have a constant axis ratio, whereas 1-dim growing particles show an decreasing axis ratio vs. size behaviour. For both, the 1-dim and 2-dim particles, the scatter decreases vs. size.

References

Baschek, B. R., R. Schefold, M. Wüest, E. Barthazy, 2002. Influence of embedded convection on microphysics of precipitation. 11th Conference on Cloud Physics, AMS, Ogden (2002).

Barthazy, E., and R. Schefold, 2001. A new ground-based optical instrument to measure snowflakes. 30th International Conference of Radar Meteorology, AMS, München (2001).

Fabry, F., and W. Szyrmer. 1999. Modelling of the melting Layer. Part II: Electromagnetic. J. Atmos. Sci., 56, 3593-3600.

Locatelli, J. D., and P. V. Hobbs, 1974. Fall speeds and masses of solid precipitation particles. J. Geophys. Res., 79, 2185.

Magono, C, and C. W. Lee, 1966. Meteorological classification of natural snow crystals. Pp. 321-355. J. Fac. Sci., Vol. II, No. 4 of VII. Hokkaido University, Japan.

Mosimann, L, E. Weingartner, and A. Waldvogel, 1994. An Analysis of accreted drop sizes and mass on rimed snow crystals. J. Atmos. Sci., 51, 1548-1558.

Schaefer, V.J. 1956. The preparation of snow crystal replicas. Weatherwise, 93, 239-24.

Vivekanandan, J., R. Raghaven and V.N. Bringi, 1993: Polarimetric radar modelling of mixtures of precipitation particles. IEEE Trans.on Geoscience and Remote Sensing, 31, No. 5, 1017-1030.

Zikmunda, J, 1972. Fall velocities of spatial crystals and aggregates. J. Atmos. Sci., 29, 1511.